

This work was written as part of one of the author's official duties as an Employee of the United States Government and is therefore a work of the United States Government. In accordance with 17 U.S.C. 105, no copyright protection is available for such works under U.S. Law. Access to this work was provided by the University of Maryland, Baltimore County (UMBC) ScholarWorks@UMBC digital repository on the Maryland Shared Open Access (MD-SOAR) platform.

Please provide feedback

Please support the ScholarWorks@UMBC repository by emailing [scholarworks-group@umbc.edu](mailto:scholarworks-group@umbc.edu) and telling us what having access to this work means to you and why it's important to you. Thank you.



## Full length article

# Collagen hydrogel confinement of Amyloid- $\beta$ ( $A\beta$ ) accelerates aggregation and reduces cytotoxic effects

Laura W. Simpson<sup>a</sup>, Gregory L. Szeto<sup>a,b</sup>, Hacene Boukari<sup>c</sup>, Theresa A. Good<sup>d</sup>,  
Jennie B. Leach<sup>a,\*</sup>

<sup>a</sup> Department of Chemical, Biochemical and Environmental Engineering, University of Maryland Baltimore County, Baltimore, MD, United States

<sup>b</sup> Marlene and Stewart Greenebaum Comprehensive Cancer Center, University of Maryland, Baltimore, Maryland, United States

<sup>c</sup> Division of Physical and Computational Sciences, Delaware State University, Dover, Delaware, United States

<sup>d</sup> Division of Molecular and Cellular Biosciences, National Science Foundation, Alexandria, Virginia, United States

## ARTICLE INFO

## Article history:

Received 18 June 2019

Revised 18 May 2020

Accepted 19 May 2020

Available online 25 May 2020

## Keywords:

Alzheimer's disease

Beta amyloid

Aggregation

Hydrogel

Confinement

## ABSTRACT

Alzheimer's disease (AD) is the most common form of dementia and is associated with the accumulation of amyloid- $\beta$  ( $A\beta$ ), a peptide whose aggregation has been associated with neurotoxicity. Drugs targeting  $A\beta$  have shown great promise in 2D in vitro models and mouse models, yet preclinical and clinical trials for AD have been highly disappointing. We propose that current in vitro culture systems for discovering and developing AD drugs have significant limitations; specifically, that  $A\beta$  aggregation is vastly different in these 2D cultures carried out on flat plastic or glass substrates vs. in a 3D environment, such as brain tissue, where  $A\beta$  confinement alters aggregation kinetics and thermodynamics. In this work, we identified attenuation of  $A\beta$  cytotoxicity in 3D hydrogel culture compared to 2D cell culture. We investigated  $A\beta$  structure and aggregation in solution vs. hydrogel using Transmission Electron Microscopy (TEM), Fluorescence Correlation Spectroscopy (FCS), and Thioflavin T (ThT) assays. Our results reveal that the equilibrium is shifted to stable extended  $\beta$ -sheet (ThT positive) aggregates in hydrogels and away from the relatively unstable/unstructured presumed toxic oligomeric  $A\beta$  species in solution. Volume exclusion imparted by hydrogel confinement stabilizes unfolded, presumably toxic species, promoting stable extended  $\beta$ -sheet fibrils.

## Statement of Significance

Alzheimer's disease (AD) is a devastating disease and has been studied for over 100 years. Yet, no cure exists and only 5 prescription drugs are FDA-approved to temporarily treat the AD symptoms of declining brain functions related to thinking and memory. Why don't we have more effective treatments to cure AD or relieve AD symptoms? We propose that current culture methods based upon cells cultured on flat, stiff substrates have significant limitations for discovering and developing AD drugs. This study provides strong evidence that AD drugs should be tested in 3D culture systems as a step along the development pathway towards new, more effective drugs to treat AD.

© 2020 Acta Materialia Inc. Published by Elsevier Ltd. All rights reserved.

## 1. Introduction

Amyloids are defined as abnormal fibrous, extracellular, protein aggregates that accumulate in organs throughout the body. Na-

\* Corresponding author at: UMBC, Chemical, Biochemical & Environmental Engineering, 1000 Hilltop Circle, Baltimore, MD 21250, United States.

E-mail addresses: [lwalk2@umbc.edu](mailto:lwalk2@umbc.edu) (L.W. Simpson), [gszeto@umbc.edu](mailto:gszeto@umbc.edu) (G.L. Szeto), [hboukari@desu.edu](mailto:hboukari@desu.edu) (H. Boukari), [tgood@nsf.gov](mailto:tgood@nsf.gov) (T.A. Good), [jleach@umbc.edu](mailto:jleach@umbc.edu) (J.B. Leach).

tive proteins misfold, and intrinsically-disordered proteins fold predominantly into a  $\beta$ -sheet conformation. Under certain conditions the  $\beta$ -sheet structure extends, leading to the formation of amyloid fibrils; this aggregation process either leads to loss of function of the native protein or gain of toxic function of the aggregated amyloid protein. There are currently 37 human amyloid proteins identified that are linked to neurodegenerative diseases and amyloidosis diseases [1,2]. Alzheimer's disease (AD) is the most common form of dementia [3] and is associated with the accumulation of amyloid- $\beta$  ( $A\beta$ ), and intrinsically disordered peptide between 39

and 45 amino acids long in its native form, whose aggregation has been associated with neurotoxicity in AD [4].

Since the first studies demonstrating a genetic link between A $\beta$  and early-onset AD [5], investigators have targeted A $\beta$  as a potential therapeutic strategy. Neurology has the third highest number of medications in drug development, yet there are only four unique drugs approved by the FDA for the treatment of AD [6]. Between 2002 and 2012 there were 413 clinical trials for AD. During that time only one drug was licensed by the FDA, a 99.6% failure rate [7]. Many AD drugs are A $\beta$  targeting antibodies that demonstrated promise in pre-clinical trials and mouse models yet failed to show efficacy in human patients [8,9].

There are a number of possible causes for the failure of A $\beta$  targeting drugs in clinical trials. A $\beta$  may not be causative in AD, but instead may simply be a side-product of the disease progression. The clinical trial design may be faulty in that drug intervention is administered in late-stage AD while A $\beta$  toxic effects occur significantly before (potentially decades before) the onset of symptoms. Clinical endpoints are subjective, making it difficult to determine the efficacy of any intervention. Alternatively, the 2D tissue culture models used to screen drugs for their ability to attenuate A $\beta$  toxicity are poor models for the in vivo 3D environment. Some or all of the above hypotheses may be valid; however, in this study, we set out to test the last hypothesis, that 2D tissue culture models are a poor model for A $\beta$  toxicity testing.

In vitro models typically culture cells on a 2D surface to study the cellular response to A $\beta$  [10–15]. However, 3D biomaterial scaffolds promote stem cell differentiation, cellular binding, and cell signaling that better represent in vivo cell behaviors compared to 2D cultures [16–24]. There is a growing trend across all of biotechnology and biopharmaceutical discovery teams to use 3D models of tissue as opposed to 2D tissue culture models, with remarkably good results [25–27]. 3D AD models have begun to be used to model the human cellular aspects that mouse models inherently cannot. [28–31]. Some of these 3D models have even used iPSCs taken from an AD patient and differentiated them into neurons that produced A $\beta$  and eventually tau tangles [30–32]. However, these models have yet to be used routinely for drug testing.

3D environments such as collagen hydrogels used in tissue culture models form a confined space that excludes solvent volume from soluble macromolecules [33–35]. Volume exclusion reduces the space available to an unfolded protein, thereby shifting the equilibrium towards a more compact protein conformation. For most proteins, the native state is a compact conformation [36–42]. However, with intrinsically disordered proteins and other aggregation-prone proteins, confinement promotes rapid aggregation [43–50]. Even for free, uncrosslinked crowding materials, the solvent exclusion effect has been observed experimentally [45,47] and predicted from simulation [51,52]. However, whether this effect leads to amorphous (off-pathway) aggregation [53,54], or stabilization of on-pathway intermediates [55], is unclear as conflicting results have been reported [56]. Further, for hydrogels used as cell scaffolds (e.g., collagen) the influence of 3D environments on protein structure and aggregation is equally unclear.

From studies carried out in solution and 2D culture models, we know that A $\beta$  aggregation is intimately tied to its cytotoxicity. Unstructured A $\beta$  monomers associate with each other, forming unstable oligomers that are associated with neuronal toxicity [57–61]. Fibrils and other protofibril structures are thought to be less toxic [61–63]. While it is commonly held that the unstable toxic oligomers are an “on pathway” intermediate, there are some dissenting opinions [64]. Thus, a priori, it is difficult to predict the effect of 3D confined environments on the relative distribution of A $\beta$  structures associated with aggregation and toxicity.

In this work, we tested the hypothesis that A $\beta$  toxicity is altered for cells cultured in 3D hydrogels vs. 2D cell culture plates.

We show that A $\beta$  aggregates more readily in the 3D confined environment of a hydrogel. We suggest the differences in toxicity between 2D and 3D cultures are a result in a shift in chemical equilibrium from oligomer to fibril, and from toxic to less toxic species, in these environments. Finally, we propose that some clinical trials of AD drugs fail as a result of the differences in the biophysical environment in 2D culture and the in vivo environment; therefore, we suggest that future A $\beta$  toxicity studies be conducted in 3D hydrogel cultures so that the biophysics of A $\beta$  aggregation better approximates the in vivo scenario.

## 2. Materials and methods

### 2.1. Beta-Amyloid preparation

Human beta-amyloid (1–42) (A $\beta$ ) and scrambled A $\beta$  (1–42) (Scr A $\beta$ ) (AIAEGDSHVLKEGAYMEIFDVQGHVFGGKIFRVVDLGSHNVA) was purchased from AnaSpec (Fremont, CA) and Genscript (Piscataway, NJ). HiLyte 488-labeled A $\beta$  (1–42) (HiLyte A $\beta$ ) and FAM-labeled scrambled A $\beta$  (1–42) (FAM Scr A $\beta$ ) were purchased from AnaSpec (Fremont, CA). All other unspecified reagents were purchased from Sigma Aldrich (St. Louis, MO) or Thermo Fisher Scientific (Waltham, MA).

In order to break any existing  $\beta$ -sheet structures and monomerize the protein, lyophilized A $\beta$  was pretreated with hexafluoro-2-propanol at a concentration of 1 mg/ml for 40 mins until A $\beta$  was fully dissolved. A $\beta$  aliquots were transferred into glass scintillation vials, and hexafluoro-2-propanol was evaporated under vacuum overnight. Aliquots of dried peptide film were stored at –20 °C. For an experiment, an A $\beta$  aliquot was dissolved in freshly-made and filtered 60 mM NaOH and allowed to dissolve for 2 mins at room temperature. Tissue culture grade water was then added, and the vial was sonicated for 5 mins. The A $\beta$  solution was then filtered with a 0.2  $\mu$ m pore, 4 mm diameter syringe filter. Sterile phosphate buffered saline (PBS) was then added to the A $\beta$  monomer solution yielding a final concentration of 222  $\mu$ M with the NaOH:water:PBS ratio of 2:7:1. The A $\beta$  solution was used immediately after preparation at a final concentration of 20  $\mu$ M unless stated otherwise. HiLyte A $\beta$  and FAM Scr A $\beta$  were prepared in the same NaOH:water:PBS ratio solution to a stock A $\beta$  concentration of 10  $\mu$ M. All FCS experiments used 250 nM fluorophore-labeled A $\beta$ .

### 2.2. Hydrogel preparation

Rat tail collagen type I hydrogels were prepared to final concentrations ranging from 0.5 to 2 mg/ml. Cold 5x Dulbecco's Modified Eagle's Medium (DMEM) without phenol red, 7.5% sodium bicarbonate, sterile deionized water, and collagen were combined. Other experimental additives were mixed into the cold hydrogel solution and in Section 2.3 Live/Dead Assay, PC12 cells were mixed in. The cold hydrogel solution (containing cells) was pipetted into wells. The samples were placed in a culture incubator for 20 mins to allow for gelation to generate 3D substrates. Warm serum free culture medium was then added to the wells.

### 2.3. Cell culture

PC12 cells (ATCC, Manassas, VA) (CRL-1721TM) are non-adherent to tissue plastic; therefore, were cultured on collagen-coated flasks at 5  $\mu$ g/cm<sup>2</sup>. Growth medium consisted of DMEM/F12 with L-glutamine and without phenol red, supplemented with 10% inactivated horse serum, 5% fetal bovine serum, and 20  $\mu$ g/ml gentamicin. Experimental medium consisted of Neurobasal medium without phenol red, supplemented with 1% B27 and 10  $\mu$ g/ml gentamicin. Phenol red and serum were avoided

in the experiments because they are inhibitors of A $\beta$  aggregation [65,66].

#### 2.4. Live/Dead assay

PC12 cells were collected by trypsin treatment, and viability was determined by trypan blue staining. To remove serum, cells were resuspended in experimental medium, pelleted then resuspended again in experimental media. In a black-walled clear-bottom tissue culture treated 96-well plate, wells for 2D culture were collagen coated at 5  $\mu\text{g}/\text{cm}^2$ , and then PC12 cells were seeded at  $15 \times 10^3$  cell/ $\text{cm}^2$ . For the 3D hydrogels, PC12 cells and (in A $\beta$  conditions) pre-treated, monomeric A $\beta$  were mixed into cold pre-gelled collagen (1 mg/ml) solution at a concentration of 500 cell/ $\mu\text{l}$  and 20  $\mu\text{M}$  respectively. The solution was then pipetted (30  $\mu\text{l}$ ) into the well plate and allowed to solidify. All wells were incubated in 200  $\mu\text{l}$  warmed experimental medium; 2D culture conditions' medium contained 20  $\mu\text{M}$  pre-treated, monomeric A $\beta$ . The medium was not changed during the 72 h experiment.

To determine cell viability, the Live/Dead mammalian cell kit (Invitrogen, Carlsbad, CA) was applied at a concentration of 4  $\mu\text{M}$  Calcein AM (green-fluorescing live cell reporter) and 9  $\mu\text{M}$  Ethidium homodimer-1 (EthD) (red-fluorescing dead cell reporter) and incubated at 37  $^\circ\text{C}$  for 30 min. Images were taken on an IX81 Olympus inverted fluorescent microscope. A minimum of 100 cells were counted per well, two images per well, three wells per condition. The data is presented as percent viability, averaged between the three replicate experiments.

#### 2.5. Thioflavin T

A black-walled clear-bottom 384 well plate (Costar) was sterilized under UV light for 15 min in a laminar flow hood. UltraPure grade Thioflavin T (ThT) (AnaSpec, Fremont, CA) was dissolved in deionized water at a concentration of 1 mM then filter-sterilized. Wells for 2D and 3D samples were prepared as above, but containing 20  $\mu\text{M}$  ThT mixed into the cold pre-gelled collagen solution. The collagen hydrogels were prepared at 1 mg/ml in all experiments except for Fig. 6.c. where collagen concentration is varied between 0.5 – 2 mg/ml. The wells were sealed with black TopSeal-A membranes to prevent evaporation. The ThT experiment was analyzed on a Spectra Max M5 (Molecular Devices, San Jose, CA) spectrophotometer set to ex. 450 nm, em. 480 nm, at 37  $^\circ\text{C}$ , taking reads every 30 mins for 72 hrs, reading from the bottom of the plate. Replicates were averaged, A $\beta$  data was corrected with ThT control data (data not shown), and corrected curves were normalized. Due to the stochastic nature of aggregation, representative curves are presented here.

#### 2.6. Transmission electron microscopy

Samples for transmission electron microscopy (TEM) imaging were prepared as follows. Reconstituted 222  $\mu\text{M}$  A $\beta$  was diluted to 20  $\mu\text{M}$  in experimental media. Timepoints were taken at 0, 24, 48, and 72 hrs. Samples were prepared on copper-supported carbon formvar grids (FCF200-Cu-TB) (EMS, Hatfield, PA) and stained with 0.2% uranyl acetate. Grids were imaged at 180–220 kx on an FEI Morgagni M268 100 kV Transmission Electron Microscope equipped with a Gatan Orius CCD camera.

#### 2.7. Fluorescence correlation spectroscopy

##### 2.7.1. Theory

Fluorescence Correlation Spectroscopy (FCS) measures the fluctuations of fluorescence in a small, optically-defined confocal volume ( $\sim 10^{-15}$  liter). These fluctuations are typically attributed to the

fluorescent particles moving in and out of the volume with a statistical average residence time,  $\tau_D$ . The residence time is proportional to the hydrodynamic radius ( $R_H$ ) of the molecule. The fluctuations of detected photons inform the autocorrelation,  $G(\tau)$ , function defined as

$$G(\tau) = \frac{\delta I(t + \tau)\delta I(t)}{I(t)^2}$$

Where  $\delta I(t) = I(t) - \langle I(t) \rangle$  is the fluorescence fluctuation determined from the measured fluorescence intensity,  $I(t)$ , at time  $t$ , and the average intensity,  $\langle I(t) \rangle$ , over the period of measurement. The excitation laser, which is focused, is assumed to have a 3D Gaussian profile, with a characteristic radial dimension ( $w_0$ ) and a characteristic axial dimension ( $z_0$ ). For a solution of  $n$  noninteracting, freely diffusing fluorescent species  $G(\tau)$  is given by:

$$G(\tau) = \sum_{i=1}^n b_i \left( \frac{1}{1 + \frac{\tau}{\tau_{D_i}}} \right) \left[ \frac{1}{1 + \left( \frac{w_0}{z_0} \right)^2 \frac{\tau}{\tau_{D_i}}} \right]^{1/2}$$

$$\tau_{D_i} = \frac{w_0^2}{4D_i}$$

Here the  $D_i$  values are the  $n$  different values of diffusion constants and  $b_i$  are the relative fractions in brightness of these species. In practice, the radial and axial dimensions were determined using Alexa 488 dye in water where the diffusion coefficient (430  $\mu\text{m}^2/\text{s}$ ) is known and was used to estimate the excitation volume for a 3D Gaussian beam [67].

##### 2.7.2. Methods

Neurobasal medium was used in preparing solution samples and contained 20  $\mu\text{M}$  A $\beta$  and 250 nM HiLyte A $\beta$ . Collagen hydrogels (1 mg/ml) were prepared as described in Section 2.2 with the addition of 20  $\mu\text{M}$  A $\beta$  and 250 nM HiLyte A $\beta$  into the cold pre-gel solution, then pipetted (60  $\mu\text{l}$ ) into 0.8 mm deep, 9 mm diameter hybridization chambers (PerkinElmer, Waltham, MA) on a borosilicate cover glass. Control samples were tested with 20  $\mu\text{M}$  Scr A $\beta$  and 250 nM FAM Scr A $\beta$ . The beam was set at 10–50  $\mu\text{m}$  into the depth of the hydrogel and solution samples to avoid aggregates that had settled. Various random locations within the hydrogel were analyzed to account for possible spatial heterogeneities.

The FCS measurements were performed using an Alba-FFS microscope-based system from ISS Inc. (Champaign, IL). The system is composed of: an Olympus IX81 inverted microscope equipped with a 60X/1.35NA oil immersion objective lens, a Prior Pro-stage, three different lasers (450 nm, 488 nm, and 532 nm), two Hamamatsu photon multiplier tubes (PMTs) for photodetection, and two sets of computer-controlled scanned mirrors for imaging. In these measurements, only the 488-nm diode laser was used for excitation of the fluorophores Alexa 488 or fluorescently-labeled A $\beta$ , and the emitted fluorescence was collected through confocal detection with a pinhole ( $< 50$  nm) located in the image plane of the excited focused beam inside the sample. The emitted fluorescent beam was optically filtered further with (525/50 nm) filter and then sent to a 50/50 beam splitter for detection by two PMTs positioned in a 90-degree angle configuration. The photo-counts of both PMTs were continuously acquired and then computationally cross-correlated in order to eliminate the afterpulsing effect of a single PMT, which is typically noticeable at short delay times ( $< 10$  ms).

Using Vista Vision software, two runs were carried out back to back collecting for 3 min each to generate the correlation function  $G(\tau)$  for each sample at a time point. The two correlation functions were averaged, and the Scr A $\beta$  correlation function was fit using the one-component model to determine the diffusivity of the monomer. Further, the measured time-correlation functions for A $\beta$

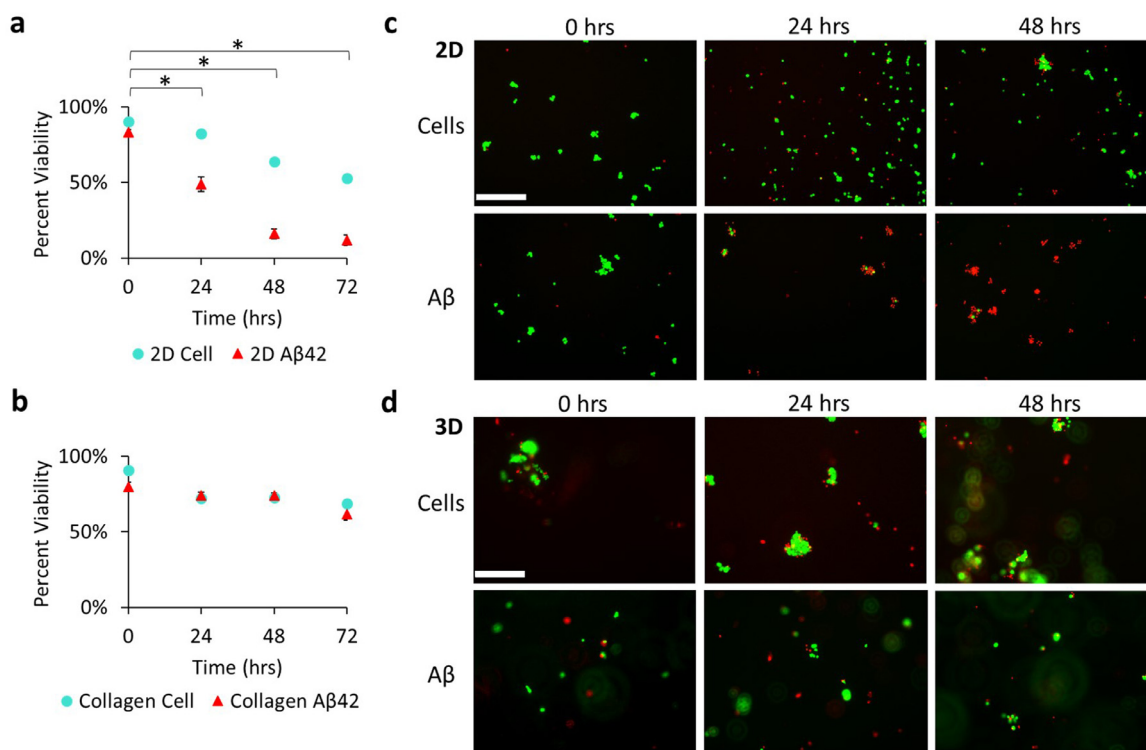


**Fig. 1.** PC12 cell percent viability in 2D and 3D culture. Using a Live/Dead assay without A $\beta$  (a & b; turquoise, ●), or with 20  $\mu$ M A $\beta$  (a & b; red, ▲). Cells were cultured on 2D plates coated with collagen I (a), or encapsulated within a 1 mg/ml collagen hydrogel (b). Cells were imaged in 2D (c) and 3D (d), without A $\beta$  and with A $\beta$ , where live cells appear green (Calcein-AM) and dead cells appear red (EthD). Significant differences were seen in (a) 2D culture in the presence of A $\beta$  at 24, 48, and 72 hrs signified by (\*). Statistics used  $n = 4$ . P values at significantly different times in 2D culture: 24 hrs (0.004), 48 hrs (<0.001), and 72 hrs (<0.001). Error bars are the percent error of the mean population. Scale bar is 200  $\mu$ m; all micrographs are the same magnification. (For interpretation of the references to colour in this figure legend, the reader is referred to the web version of this article.)

were fit using the 2-component model where the size of species 1 was held constant at monomer diffusivity in order to derive the average aggregate diffusivity population of the second species. Additional refinement for fitting the correlation functions were also performed with the Maximum Entropy Method FCS (MEMFCS) thanks to a code gifted by Dr. S. Maiti (Tata Institute of Fundamental Research), allowing us to obtain the heterogeneous distribution of aggregate diffusivities at each time point [68].

Small molecules have a short delay time because they diffuse quickly through the volume, whereas large molecules have a long delay time because of their relatively slow diffusion through the volume. The 2-component model is intended to model two distinct molecular species in solution. For our samples, we held the monomer diffusivity constant as species 1 where the average diffusivity of aggregated species was identified by solving for species 2.

Fluorophore labeling of A $\beta$  monomers inhibits aggregation due to the bulky groups sterically preventing proper monomer to monomer stacking [69]. Therefore, we used a ratio of 1:80 HiLyte 488-labeled A $\beta$  to unlabeled A $\beta$ , and FAM-labeled Scr A $\beta$  to unlabeled Scr A $\beta$ , to allow unhindered  $\beta$ -sheet stacking. Nanomolar fluorophore concentrations are also preferable in FCS in order for the detectors to monitor few individual fluorescent molecules in the confocal volume, thus enhancing the signal-to-noise of the fluctuations.

## 2.8. Statistical analysis

Data were analyzed for statistical significance with Prism v8 software (GraphPad). Cell viability data were analyzed with a general ANOVA with a post Tukey pairwise test which determined significant deviation from the population mean with a p-value

<0.05 with 95% confidence. Error bars are the percent error of the mean population. The raw FCS experimental  $G(\tau)$  curves, the 2-component model calculated  $G(\tau)$  curves, and the MEMFCS calculated  $G(\tau)$  curves were analyzed for significance using the 2-sample Kolmogorov-Smirnov test with 95% confidence.

## 3. Results

### 3.1. Toxicity of A $\beta$ in 2D and 3D cultures

We initially hypothesized that 3D hydrogels would be better models in which to test A $\beta$  toxicity because neurons have a more in vivo like phenotype in 3D compared to 2D cultures [23,70]. As such, we expected A $\beta$  to be more toxic to cells in 3D than in 2D. To begin to test this hypothesis, we examined the toxicity of PC12 cells when dosed with A $\beta$  (pretreated to remove  $\beta$ -sheet structure) in both 2D and 3D collagen over a 72 hr period (Fig 1).

We acknowledge that the percent viability decreases for all samples over time, but it is important to note that the medium was not changed in order to better mimic the evolving population of A $\beta$  species measured in the ThT and FCS experiments. Over 72 hrs, it is likely that cell waste accumulates and nutrients are depleted, thus explaining the decrease in cell viability in all conditions. The number of viable cells cultured in 2D with 20 M pretreated A $\beta$  decreased significantly by 24 hrs where the cell viability was 49% (p-value 0.004); at 48 hrs and 72 hrs the cell viability was only 16% (p-value <0.001) and 12% (p-value <0.001) respectively (Fig. 1a). When cells were encapsulated within 3D collagen hydrogels, treatment with A $\beta$  did not affect cell viability (Fig. 1b). Representative fluorescence microscopy images of stained cells at 0 hrs, 24 hrs, and 48 hrs in 2D and 3D culture are shown in Figs. 1c and 1d respectively. In the presence of A $\beta$ , the cell death



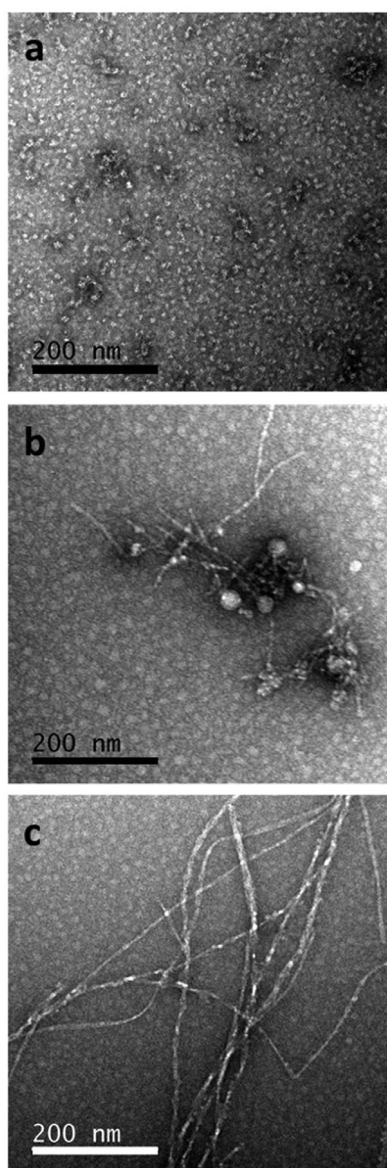


**Fig. 2.** TEM images of A $\beta$  in solution. Pretreated A $\beta$  (20  $\mu$ M) was stained with 0.2% uranyl acetate at time 0 hrs (a), 24 hrs (b), and 72 hrs (c). Scale bar is 200 nm.

(red staining) at 48 h in 2D culture is striking (Fig. 1c), while no notable increase in cell death is observed in the A $\beta$ -treated 3D cultures (Fig. 1d).

### 3.2. TEM imaging of A $\beta$ in solution

Given the well-known correlation between A $\beta$  structure or aggregation state and toxicity, we sought to confirm that the A $\beta$  used in these studies aggregated as expected and that the surprising cell viability results were not the result of some anomalous aggregation process. To this end, we performed TEM imaging of the pretreated A $\beta$  at time points after dissolution relevant to the viability studies.

Representative TEM micrographs are shown in Fig. 2. At time zero, unstructured protein globules of various sizes were identified (Fig. 2a). The smallest structures have a diameter of  $\sim$ 3.6 nm, which correlates well to the size of A $\beta$  monomer (hydrodynamic radius of 1.8 nm) [71]. Larger globular structures are 6–50 nm in diameter and lack any fibrillar structures. At 24 hrs, thin filamentous aggregates ( $\sim$ 3 nm diameter) are seen to extend from the unstructured globules (Fig. 2b). By 72 hrs, thick A $\beta$  fibrils are present

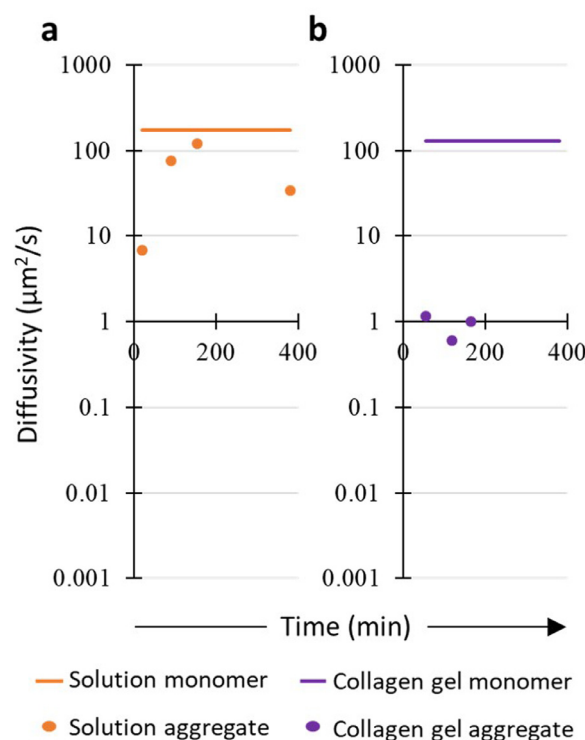


**Fig. 3.** FCS correlation functions of A $\beta$  were fit with a 2-component model. Samples of 20  $\mu$ M A $\beta$  with 250 nM HiLyte A $\beta$  in solution (a; orange,  $\bullet$ ) and in collagen hydrogel (b; purple,  $\bullet$ ) were analyzed. Species 1 was held constant at the diffusivity of the Scr A $\beta$  control assumed to be monomer (solid line). Species 2 was calculated and represents the average A $\beta$  aggregate diffusivity population ( $\bullet$ ). There is a significant difference between the 2-component calculated  $G(\tau)$  of solution and collagen gel, p-value: 0.0003 (solution  $n = 8$ ; collagen gel  $n = 7$ ). (For interpretation of the references to colour in this figure legend, the reader is referred to the web version of this article.)

and associate with each other into structures  $\sim$ 13 nm in diameter (Fig. 2c).

### 3.3. A $\beta$ aggregate diffusivities by FCS

Given the inherent challenges of imaging hydrogels using TEM, we utilized FCS to infer relative A $\beta$  aggregate size from the diffusivity of fluorescently-labeled A $\beta$  species. Diffusivity scales inversely to the radius of a particle. Therefore small diffusivity values correspond to large particles.

Non-aggregating Scr A $\beta$  was measured in solution and hydrogels as a monomer control. The diffusivity of these Scr A $\beta$  monomers in solution was determined to be 175  $\mu\text{m}^2/\text{s}$ , whereas the diffusivity in the hydrogel was 129  $\mu\text{m}^2/\text{s}$  (Fig. 3a & b). As points for comparison, the diffusivity of A $\beta$  monomer has been reported to be 180  $\mu\text{m}^2/\text{s}$  in solution and 62.3  $\mu\text{m}^2/\text{s}$  in brain tissue [72]. In solution, the diffusivity of the average A $\beta$  aggregate population (determined using the 2-component model) is  $\sim$ 9x slower than the monomer for up to 6 hrs (Fig. 3a). In hydrogels, the diffusivity of the average A $\beta$  aggregate population is  $\sim$ 150x slower than a monomer for up to 4 hrs (Fig. 3b). The 2-component calculated  $G(\tau)$  of solution is significantly different than the calculated  $G(\tau)$  of the collagen gel with a p-value of 0.0003. Additionally, the raw experimental  $G(\tau)$  of solution is significantly different from the raw experimental  $G(\tau)$  of the collagen gel with a p-value of  $<0.0001$ .

The correlation functions were also analyzed using the MEM-FCS program, which attempts to determine the distribution of size of the aggregating solutions. A distribution of multiple diffusiv-

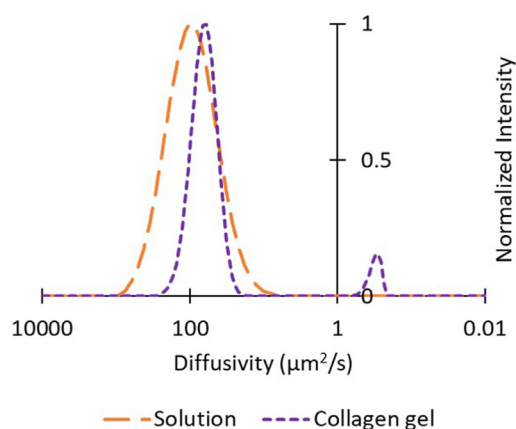


**Fig. 4.** FCS correlation function was fit using the Maximum Entropy Method program for FCS gifted by Dr. S. Maiti [68]. Solution timepoints were collected over 8 hrs; a representative curve is shown (long dash, orange). Collagen hydrogel timepoints were collected over 4 hrs; a representative curve is shown (short dash, purple). There is a significant difference between the MEMFCS calculated  $G(\tau)$  of solution and collagen gel,  $p$ -value: 0.0004 (solution  $n = 6$ ; collagen  $n = 6$ ). (For interpretation of the references to colour in this figure legend, the reader is referred to the web version of this article.)

ity populations of A $\beta$  aggregates and their relative fractions were modeled. In solution, A $\beta$  diffusivity values have a single broad distribution with an average peak diffusivity of  $90 \mu\text{m}^2/\text{s}$  (Fig. 4, solution). The peak diffusivity of A $\beta$  in solution is  $\sim 2\times$  slower than the Scr A $\beta$  diffusivity, suggesting an A $\beta$  population predominately composed of dimers. In the hydrogel, A $\beta$  has a peak diffusivity of  $60 \mu\text{m}^2/\text{s}$ , which is  $\sim 2\times$  slower than the Scr monomer ( $129 \mu\text{m}^2/\text{s}$ ). However, in contrast to the solution samples that only have one diffusivity peak, the hydrogel sample data show a small secondary diffusivity peak as early as 5 mins after addition of A $\beta$  to the hydrogel and persists throughout the measurement period (up to 4 hrs) with diffusivity values in the range of  $0.2 \mu\text{m}^2/\text{s}$ – $3 \mu\text{m}^2/\text{s}$ , or between  $650\times$  to  $45\times$  slower than Scr A $\beta$  (Fig. 4, collagen). The MEMFCS calculated  $G(\tau)$  of solution is significantly different from the collagen gel calculated  $G(\tau)$  with a  $p$ -value of 0.0004.

Both analysis methods of the FCS data indicate that A $\beta$  aggregates differently in 2D compared to 3D. Based on these data, a rough estimate of aggregate species size in 3D is  $\sim 25\times$  to  $200\times$  larger in diameter than the A $\beta$  species detected in 2D.

### 3.4. ThT fluorescence as a measure of A $\beta$ aggregation kinetics

While FCS is a powerful technique to measure diffusivities of molecules in complex media, it is difficult to get direct information on the structure or morphology of an aggregated species. Therefore, we used a ThT fluorescence assay as an additional measure of A $\beta$  aggregation.

Representative curves of ThT fluorescence vs. time are shown in Fig. 5 for A $\beta$  aggregation in solution and collagen hydrogels. In solution, fibrillar A $\beta$  aggregation (signified by ThT fluorescence) has a lag phase during the first  $\sim 20$  hrs, followed by rapid aggregation (Fig. 5, orange). In hydrogels, however, fibrillar aggregation does not show a lag phase, and instead, fluorescence steadily increases from the initiation of the experiment (Fig. 5, purple). Depending upon the supplier and lot of A $\beta$  tested, lag time and fluorescence intensity varied, but the qualitative differences between fibril A $\beta$  aggregation in solution and the collagen hydrogel persisted; fibril aggregation was accelerated in the hydrogel compared to the solution.

In solution samples, the duration of the aggregation lag phase varied with A $\beta$  concentration: greater A $\beta$  concentrations corre-

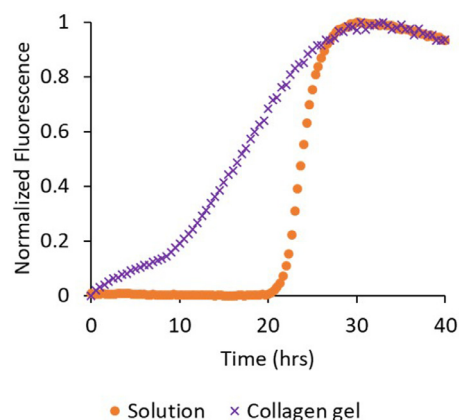


**Fig. 5.** ThT fluoresces only when bound to stacked  $\beta$ -sheet structures. Shown are representative data of ThT fluorescence due to A $\beta$  aggregation in solution (orange;  $\bullet$ ) and collagen hydrogel (purple;  $\times$ ). (For interpretation of the references to colour in this figure legend, the reader is referred to the web version of this article.)

lated with shorter lag phases of fibril aggregation in solution. The lag phase lasted 7.5 hrs for  $10 \mu\text{M}$  A $\beta$ , 4 hrs for  $25 \mu\text{M}$  A $\beta$ , and only 1 h for  $50 \mu\text{M}$  A $\beta$  (Fig. 6a). This effect was also noted for collagen hydrogels ( $1 \text{ mg/ml}$ ), but on a much faster timescale: the lag phase was 1 h for  $10 \mu\text{M}$  A $\beta$ , and nonexistent for  $25 \mu\text{M}$  and  $50 \mu\text{M}$  A $\beta$  (Fig. 6b). The rate of fibril aggregation ( $20 \mu\text{M}$  A $\beta$ ) was also influenced by the collagen concentration of the hydrogel: at collagen concentrations of 0.5, 1, 1.5 and  $2 \text{ mg/ml}$ , the lag phases were observed to be 13.5 hrs, 9.5 hrs, 9 hrs, and 6.5 hrs, respectively (Fig. 6c).

The drop in ThT fluorescence for high concentrations of Abeta is associated with ThT quenching and/or inner filter effects. We maintained lower concentrations of both Abeta and ThT in the rest of the experiments to minimize this effect. The A $\beta$  protein aggregation is highly stochastic and has variation in aggregation rate between manufacturing lots (data not shown). The experiments conducted for Fig. 6a and b used the same lot and were run at the same time from the same A $\beta$  aliquot. The experiments for 6c were conducted at a later time with a different lot that aggregated more slowly. The purpose of Fig. 6c is not to be compared to the data of Fig. 6a and b, but to simply show that the change in collagen hydrogel concentration, alters the A $\beta$  aggregation lag time. Despite varying aggregation lag phase from lot to lot, we consistently saw the same kinetic trends in solution compared to in collagen hydrogel.

## 4. Discussion

For almost three decades, researchers have recognized a link between A $\beta$  and AD and pursued drug candidates capable of preventing A $\beta$  aggregation as new therapeutic strategies for AD [73–75]. These interactions were measured in cell culture experiments but were associated with little or no efficacy in pre-clinical testing and clinical trials [7,9,76–79].

There is a growing appreciation that cells grown in vitro, on rigid polystyrene tissue culture surfaces, behave very differently than cells in vivo, and that the stiffness of the surface upon which cells are grown can have profound epigenetic effects on cells that influence their phenotype [80,81]. In addition, many investigators have observed that morphologies of neuronal cells are strikingly more similar to those expressed in vivo in 3D vs. 2D culture [22,23,82,83]. Thus, the use of 3D cell culture models for AD drug development may lead to a more positive correlation between successes in vitro and successes in clinical outcomes.

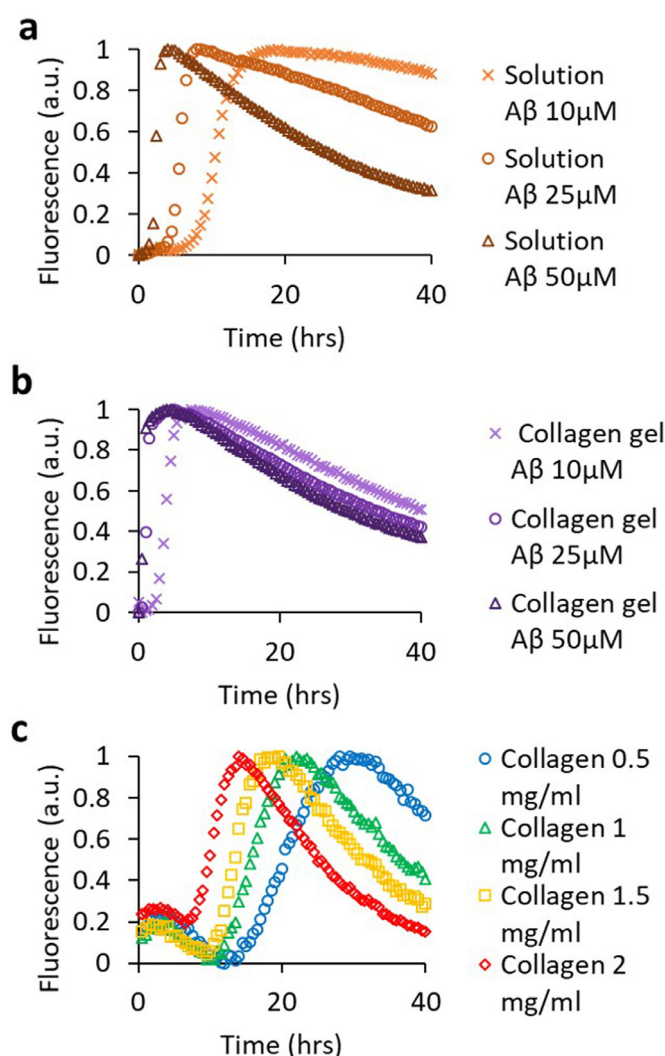


**Fig. 6.** Aβ and collagen concentration impact ThT aggregation kinetics. ThT aggregation kinetics comparing Aβ concentrations (10 μM, light x; 25 μM, medium o; 50 μM, dark Δ) in solution (a, orange) and collagen hydrogel at 1 mg/ml (b, purple). In c, Aβ (20 μM) aggregation kinetics is compared in hydrogels with collagen concentrations of 0.5 mg/ml (blue; o), 1 mg/ml (green; Δ), 1.5 mg/ml (yellow; □), and 2 mg/ml (red; ◇). (For interpretation of the references to colour in this figure legend, the reader is referred to the web version of this article.)

The preponderance of literature reports indicates that Aβ is toxic to cells in culture only when aggregated and that it is the oligomeric or intermediate-sized aggregation species that are the most toxic species, with large fibril aggregates being less toxic [57,62]. These findings were reported for cells in traditional culture on flat rigid substrates such as polystyrene or glass. To our knowledge, no one has explored Aβ aggregation kinetics and cellular toxicity in a 3D cell culture model.

In the work presented here, our 2D cell culture of PC12 cells demonstrated the expected cytotoxic nature of Aβ aggregates. However, when PC12 cells and Aβ were encapsulated within 3D collagen hydrogels, the cytotoxic effects were attenuated. We supposed that this effect could be due to one of two effects, either (1) the 3D environment altered the PC12 cells, making them less susceptible to Aβ, or (2) the 3D environment altered the aggregation of Aβ. Given that PC12 cells and other neuron-like cells take on a phenotype more closely associated with an in vivo neuron in 3D [22,23,84], we assumed that our first hypothesis was less probable.

Therefore, in this work, we set out to investigate how the 3D collagen hydrogel environment affects Aβ structure and aggregation.

We used a combination of biophysical methods to investigate Aβ structure and aggregation both in solution and in the 3D collagen hydrogel. TEM micrographs of pretreated Aβ that underwent aggregation in solution confirm that the structures seen during our experiments are typical of those seen by others [85,86]. The pretreatment process removed any observable fibril or protofibril structures (Fig. 2a). FCS and ThT measurements at these early time points (<24 hrs) suggest that only small, rapidly diffusing species remained after Aβ pretreatment; the samples were devoid of any extended β-sheet structures (Figs. 3a, 4, and 5, respectively). These results are consistent with literature reports for Aβ pretreatment via this method [59,71]. Shortly after the dissolution of Aβ, the Aβ in solution appeared to form dimer or similar diffusing species (Fig. 4, solution), and other somewhat larger aggregated species with diffusivity values on the order of 20 μm<sup>2</sup>/s (Fig. 3a). The observance of monomers and dimers in equilibrium at early stages of aggregation of Aβ in solution has been seen via other methods including chromatography [87,88] and hydrogen exchange mass spectrometry and others [89,90]. The observance of larger aggregated species in Aβ solutions that are non-fibril (i.e., they do not bind ThT; Fig. 5), such as the more slowly diffusing species seen in FCS (Fig. 3a) and TEM micrographs (Fig. 2b), is consistent with the formation of the toxic oligomer species. While there is considerable debate concerning the actual size and structure of the most toxic species of aggregated Aβ, most consider that this species is smaller than a fibril [91], and by some accounts, the diffusivity of the toxic Aβ species is on the order of 20 μm<sup>2</sup>/s [63,92]. Aβ aggregated for 72 h shows typical fibril structures via TEM (Fig. 1c), that bind ThT (Fig. 5), as would be expected for large extended β-sheet structures [93]. Given the typical aggregation pathway, we observed of Aβ in solution – one that included detectable oligomers that are suggested to be the most toxic species – the viability results observed in 2D cell culture (Fig. 1a & 1c) were expected.

The same careful biophysical examination of Aβ aggregation in 3D collagen hydrogels demonstrates that aggregation does not proceed through the same pathway as in solutions. Even at early times during aggregation, no slowly diffusing species (diffusivity ~20 μm<sup>2</sup>/s) were observed (Figs. 3b,4). At these early times during aggregation, only a small unaggregated species and a very large/slow diffusing species were observed; the larger species diffused 10x to 100x more slowly than the oligomer observed in solution (Figs. 3,4). Given the ThT fluorescence seen even at these early times (Fig. 5), this larger species may be a fibril form of Aβ. We hypothesize that we did not observe any notable Aβ toxicity in 3D culture because Aβ aggregation proceeded through a pathway that did not include the formation of any detectable oligomeric species that are typically associated with Aβ toxicity.

While we are not aware of any other studies of Aβ aggregation in a 3D environment, the effect of crowding and confinement on protein folding and aggregation has been previously studied [41,48]. Biomaterial scaffolds are composed of self-associating or crosslinked structures that exert an excluded volume effect on soluble molecules that are entrapped within. The excluded volume effect increases the local concentration of soluble molecules, increasing the chance of protein-protein interactions. The reduced volume also confines the available space a protein may use to fold, promoting a more compact, low entropy conformation. Uncrosslinked crowding molecules such as polyethylene glycol (PEG), Ficoll, and bovine serum albumin stabilize protein folding into functional states or accelerate aggregation in aggregation-prone proteins (e.g., lysozyme, α-synuclein, and β2-microglobulin) [44,45,48]. Alternatively, crowding molecules stabilize globular monomers of human islet amyloid polypeptide that are non-toxic, inhibiting the toxic



fibrillization pathway associated with type-2 diabetes [94]. Confinement has a greater stabilization effect than crowding but is seldom used to study the biophysics of proteins [39,95,96]. We suggest that in our studies, the confinement provided by the 3D collagen hydrogel resulted in increased A $\beta$ -A $\beta$  interactions, thus leading to the observed faster aggregation kinetics and the lack of slower diffusing species. If this were the case, then we would expect to see that higher concentrations of A $\beta$  shortened the lag time to the onset of rapid aggregation due to the greater probability of nucleation of aggregation. This is indeed what we observed (Fig. 6a and b). At every concentration tested, the lag phase until the onset of rapid aggregation was significantly shorter in 3D environments and shorter at higher A $\beta$  concentrations. The acceleration of aggregation of A $\beta$  with increasing concentrations of collagen in the 3D hydrogels (Fig. 6c) is consistent with the hypothesis as well; higher collagen concentrations would lead to smaller void spaces in the 3D collagen hydrogel, thus greater confinement, increased A $\beta$ -A $\beta$  interactions, and acceleration of A $\beta$  aggregation.

The above hypothesis assumes that there are no direct physical interactions between A $\beta$  and collagen. As a charged protein with significant hydrophobic content, it is possible that collagen may provide additional A $\beta$  nucleation sites, resulting in shortened lag times in collagen gel vs solution. Once A $\beta$  aggregation is nucleated, the A $\beta$  structures become more hydrophobic as they grow from soluble monomers into larger insoluble fibrils. The net result of these collagen-A $\beta$  interactions could also contribute to the trends seen in Fig. 5 and 6: with increased A $\beta$  and/or collagen concentration, both A $\beta$  nucleation (lag phase) and aggregation (slope of the rise in ThT fluorescence) increase. However, such collagen-A $\beta$  interactions would suggest that the FCS data shown in Fig. 6 may be skewed to favor the more hydrophilic species that exist within the collagen gel. In another work, we tested a series of hydrogel types with varying hydrophilicity, charge content, and mesh size [97]. All gel types attenuated A $\beta$  toxicity, but the nucleation and aggregation kinetics that were measured in collagen gels were slower than in either agarose or crosslinked PEG, suggesting that confinement may be more important than a specific collagen-A $\beta$  interaction. Additional experiments designed to test the independent effects of gel hydrophobicity, charge content and mesh size are required to determine the extent to which each of these gel properties, and thus confinement vs collagen-A $\beta$  interactions influence A $\beta$  nucleation and aggregation kinetics.

When A $\beta$  aggregation is nucleated in a confined environment, the  $\beta$ -sheet structures that form are more stable vs. aggregation as free molecules in solution, resulting in faster filament growth. Such stabilization of  $\beta$ -sheet structured A $\beta$  aggregates that occurs in collagen hydrogels should result in a shift in the chemical equilibrium of aggregate species. In solution, the equilibrium composition of A $\beta$  species is expected to be a distribution of unstructured monomer-dimer – multimer species. In confined collagen hydrogels, however, we hypothesize (and our data support) that the equilibrium is shifted to stable  $\beta$ -sheet aggregates and away from the relatively unstable/unstructured presumed toxic oligomeric A $\beta$  species.

We propose that the attenuation of A $\beta$  toxicity observed in the 3D environment is due to the shift in aggregation kinetics of A $\beta$  away from the smaller toxic oligomer. However, other explanations are also plausible. Aggregated A $\beta$  species may have hindered diffusion in the semi-solid 3D collagen hydrogel, which may impede direct contact with the PC12 cells, thereby reducing toxicity. The FCS data suggest that at least at early times the A $\beta$  species do diffuse within the hydrogel. In addition, the mesh size of the 3D collagen hydrogels used in this study was  $\sim 10\ \mu\text{m}$ , one to two orders of magnitude larger than reports of sizes of A $\beta$  toxic oligomers [98,99]. Therefore, we do not conclude that hindered diffusion of A $\beta$  within the hydrogel contributed significantly to the attenua-

tion in A $\beta$  toxicity observed in 3D compared to 2D environments. It is also possible that the 3D environment resulted in some unexpected phenotypic change in the PC12 cells that we cannot rule out in the studies performed in this work.

The shift in the equilibrium of A $\beta$  species away from smaller potentially toxic species to larger extended  $\beta$ -sheet species in confined environments observed in our studies may suggest similar phenomena in vivo tissues. At the very least, our studies suggest that A $\beta$  aggregation kinetics are fundamentally different in 3D structures as compared to in the solution phase of 2D culture, making a direct translation of results from a 2D culture model to a more *in vivo*-like 3D culture model difficult. However, this relatively simple collagen hydrogel cannot recapitulate the complexity of the *in vivo* environment. We can only speculate that the high percentage of failed A $\beta$  targeting drugs in clinical trials may be due to the drug discovery models missing essential properties such as confinement and dimensionality. Many drug companies are actively using 3D cultures and various organoid types in large-scale compound screens to evaluate efficacy in pre-clinical trials [100–106]. Knowing the biophysical impact of confinement stabilizing toxic A $\beta$  aggregate species, advanced 3D *in vitro* models may be developed to investigate AD pathology and be implemented in AD drug development.

## Declaration of Competing Interest

The authors declare that they have no known competing financial interests or personal relationships that could have appeared to influence the work reported in this paper.

## Acknowledgments

The authors would like to thank Tagide deCarvalho for her assistance with TEM imaging and Dr. S. Maiti (Tata Institute of Fundamental Research) for sharing the Maximum Entropy Method program for FCS.

## Funding

This work was supported by funding from the National Science Foundation (NSF) [EAGER CBET-1447057] and the National Institute of Health (NIH) [R01GM117159]. NSF provided support for TAG to contribute to this project through their Independent Research and Development program. Any opinion, findings, and conclusions or recommendations expressed in this material are those of the author(s) and do not necessarily reflect the views of the National Science Foundation.

## References

- [1] J.D. Sipe, M.D. Benson, J.N. Buxbaum, S.I. Ikeda, G. Merlini, M.J. Saraiva, P. Westermark, Amyloid fibril proteins and amyloidosis: chemical identification and clinical classification international society of amyloidosis 2016 nomenclature guidelines, *Amyloid* 23 (4) (2016) 209–213.
- [2] F. Chiti, C.M. Dobson, Protein misfolding, amyloid formation, and human disease: a summary of progress over the last decade, *Annu. Rev. Biochem.* 86 (2017) 27–68.
- [3] F. Khan, M. Tanaka, Designing Smart Biomaterials for Tissue Engineering, *Int. J. Mol. Sci.* 19 (1) (2017) 17 <https://pubmed.ncbi.nlm.nih.gov/29267207/>.
- [4] D.M. Walsh, D.J. Selkoe, A beta oligomers - a decade of discovery, *J. Neurochem.* 101 (5) (2007) 1172–1184.
- [5] R.E. Tanzi, L. Bertram, Twenty years of the Alzheimer's disease amyloid hypothesis: a genetic perspective, *Cell* 120 (4) (2005) 545–555.
- [6] G. Long, The Biopharmaceutical Pipeline: innovative Therapies in Clinical Development, I. Analysis Group, PhRMA, 2017.
- [7] J.L. Cummings, T. Morstorf, K. Zhong, Alzheimer's disease drug-development pipeline: few candidates, frequent failures, *Alzheimers Res. Ther.* 6 (4) (2014) 37.
- [8] L.S. Schneider, F. Mangialasche, N. Andreasen, H. Feldman, E. Giacobini, R. Jones, V. Mantua, P. Mecocci, L. Pani, B. Winblad, M. Kivipelto, Clinical trials and late-stage drug development for Alzheimer's disease: an appraisal from 1984 to 2014, *J. Intern. Med.* 275 (3) (2014) 251–283.

- [9] A. Banik, R.E. Brown, J. Bamburg, D.K. Lahiri, D. Khurana, R.P. Friedland, W. Chen, Y. Ding, A. Mudher, A.L. Padjen, E. Mukaetova-Ladinska, M. Ihara, S. Srivastava, M.V. Padma Srivastava, C.L. Masters, R.N. Kalaria, A. Anand, Translation of pre-clinical studies into successful clinical trials for alzheimer's disease: what are the roadblocks and how can they be overcome? *J. Alzheimers Dis.* 47 (4) (2015) 815–843.
- [10] S. Sabo, M.P. Lambert, K. Kessey, W. Wade, G. Krafft, W.L. Klein, Interaction of beta-amyloid peptides with integrins in a human nerve cell line, *Neurosci. Lett.* 184 (1) (1995) 25–28.
- [11] Y.-P. Li, A.F. Bushnell, C.-M. Lee, L.S. Perlmutter, S.K.F. Wong,  $\beta$ -Amyloid induces apoptosis in human-derived neurotypic SH-SY5Y cells, *Brain Res.* 738 (2) (1996) 196–204.
- [12] M.P. Mattson, B. Cheng, D. Davis, K. Bryant, I. Lieberburg, R.E. Rydel, beta-Amyloid peptides destabilize calcium homeostasis and render human cortical neurons vulnerable to excitotoxicity, *J. Neurosci.* 12 (2) (1992) 376–389.
- [13] T. Kondo, K. Imamura, M. Funayama, K. Tsukita, M. Miyake, A. Ohta, K. Woltjen, M. Nakagawa, T. Asada, T. Arai, S. Kawakatsu, Y. Izumi, R. Kaji, N. Iwata, H. Inoue, iPSC-based compound screening and in vitro trials identify a synergistic anti-amyloid beta combination for alzheimer's disease, *Cell Rep.* 21 (8) (2017) 2304–2312.
- [14] S. Hilt, R. Altman, T. Kalai, I. Maezawa, Q. Gong, S. Wachsmann-Hogiu, L.W. Jin, J.C. Voss, A bifunctional anti-amyloid blocks oxidative stress and the accumulation of intraneuronal amyloid-beta, *Molecules* 23 (8) (2018).
- [15] V. Mahairaki, J. Ryu, A. Peters, Q. Chang, T. Li, T.S. Park, P.W. Burridge, C.C. Talbot Jr., L. Asnaghi, L.J. Martin, E.T. Zambidis, V.E. Koliatsos, Induced pluripotent stem cells from familial Alzheimer's disease patients differentiate into mature neurons with amyloidogenic properties, *Stem Cells Dev.* 23 (24) (2014) 2996–3010.
- [16] N.J. Hogrebe, K.J. Gooch, Direct influence of culture dimensionality on human mesenchymal stem cell differentiation at various matrix stiffnesses using a fibrous self-assembling peptide hydrogel, *J. Biomed. Mater. Res. A* 104 (9) (2016) 2356–2368.
- [17] Z. Tong, A. Solanki, A. Hamilos, O. Levy, K. Wen, X. Yin, J.M. Karp, Application of biomaterials to advance induced pluripotent stem cell research and therapy, *EMBO J.* 34 (8) (2015) 987–1008.
- [18] A.M. Hopkins, E. DeSimone, K. Chwalek, D.L. Kaplan, 3D in vitro modeling of the central nervous system, *Prog. Neurobiol.* 125 (2015) 1–25.
- [19] B.M. Baker, C.S. Chen, Deconstructing the third dimension: how 3D culture microenvironments alter cellular cues, *J. Cell Sci.* 125 (Pt 13) (2012) 3015–3024.
- [20] S.S. Ghourichae, E.M. Powell, J.B. Leach, Enhancement of human neural stem cell self-renewal in 3D hypoxic culture, *Biotechnol. Bioeng.* 114 (5) (2017) 1096–1106.
- [21] S.S. Ghourichae, J.B. Leach, The effect of hypoxia and laminin-rich substrates on the proliferative behavior of human neural stem cells, *J. Mater. Chem. B* 4 (20) (2016) 3509–3514.
- [22] S. Balasubramanian, J.A. Packard, J.B. Leach, E.M. Powell, Three-dimensional environment sustains morphological heterogeneity and promotes phenotypic progression during astrocyte development, *Tissue Eng. Part A* 22 (11–12) (2016) 885–898.
- [23] A. Ribeiro, S. Vargo, E.M. Powell, J.B. Leach, Substrate three-dimensionality induces elemental morphological transformation of sensory neurons on a physiologic timescale, *Tissue Eng. Part A* 18 (1–2) (2012) 93–102.
- [24] A. Ribeiro, S. Balasubramanian, D. Hughes, S. Vargo, E.M. Powell, J.B. Leach, beta1-Integrin cytoskeletal signaling regulates sensory neuron response to matrix dimensionality, *Neuroscience* 248 (2013) 67–78.
- [25] F. Ordikhani, S. Sheth, S.P. Zustiak, Polymeric particle-mediated molecular therapies to treat spinal cord injury, *Int. J. Pharm.* 516 (1–2) (2017) 71–81.
- [26] F. Ordikhani, S.P. Zustiak, A. Simchi, Surface Modifications of Titanium Implants by Multilayer Bioactive Coatings with Drug Delivery Potential: antimicrobial, Biological, and Drug Release Studies, *JOM* 68 (4) (2016) 1100–1108.
- [27] Y. Fang, R.M. Eglén, Three-dimensional cell cultures in drug discovery and development, *SLAS Discov.* 22 (5) (2017) 456–472.
- [28] T. Osaki, Y. Shin, V. Sivathanu, M. Campisi, R.D. Kamm, In vitro microfluidic models for neurodegenerative disorders, *Adv. Healthc. Mater.* 7 (2) (2018).
- [29] E.J. Siney, K. Kurbatskaya, S. Chatterjee, P. Prasanna, A. Mudher, S. Willaime-Morawek, Modelling neurodegenerative diseases <em>in vitro</em>: recent advances in 3D iPSC technologies, *AIMS Cell Tissue Eng.* 2 (1) (2018) 1–23.
- [30] M. Jorfi, C. D'Avanzo, R.E. Tanzi, D.Y. Kim, D. Irimia, Human neurospheroid arrays for in vitro studies of alzheimer's disease, *Sci. Rep.* 8 (1) (2018) 2450.
- [31] J. Park, I. Wetzell, I. Marriott, D. Dreau, C. D'Avanzo, D.Y. Kim, R.E. Tanzi, H. Cho, A 3D human triculture system modeling neurodegeneration and neuroinflammation in Alzheimer's disease, *Nat. Neurosci.* 21 (7) (2018) 941–951.
- [32] S.H. Choi, Y.H. Kim, M. Heibisch, C. Sliwinski, S. Lee, C. D'Avanzo, H. Chen, B. Hooli, C. Asselin, J. Muffat, J.B. Klee, C. Zhang, B.J. Wainger, M. Peitz, D.M. Kovacs, C.J. Woolf, S.L. Wagner, R.E. Tanzi, D.Y. Kim, A three-dimensional human neural cell culture model of Alzheimer's disease, *Nature* 515 (7526) (2014) 274–278.
- [33] L. Edgar, K. McNamara, T. Wong, R. Tamburrini, R. Katari, G. Orlando, Heterogeneity of scaffold biomaterials in tissue engineering, *Materials (Basel)* 9 (5) (2016).
- [34] E.S. Place, N.D. Evans, M.M. Stevens, Complexity in biomaterials for tissue engineering, *Nat. Mater.* 8 (6) (2009) 457–470.
- [35] C. Frantz, K.M. Stewart, V.M. Weaver, The extracellular matrix at a glance, *J. Cell Sci.* 123 (Pt 24) (2010) 4195–4200.
- [36] S.B. Zimmerman, A.P. Minton, Macromolecular crowding: biochemical, biophysical, and physiological consequences, *Annu. Rev. Biophys. Biomol. Struct.* 22 (1993) 27–65.
- [37] D. Hall, A.P. Minton, Macromolecular crowding: qualitative and semiquantitative successes, quantitative challenges, *Biochim. Biophys. Acta Proteins Proteom.* 1649 (2) (2003) 127–139.
- [38] M.S. Cheung, D. Klimov, D. Thirumalai, Molecular crowding enhances native state stability and refolding rates of globular proteins, *Proc. Natl. Acad. Sci. U.S.A.* 102 (13) (2005) 4753–4758.
- [39] S. Long, J. Kunkel, P. Asuri, Influence of macromolecular crowding and confinement on enzyme activity and structure under native and denaturing conditions, *Biochem. Anal. Biochem.* 07 (02) (2017).
- [40] D.K. Eggers, J.S. Valentine, Molecular confinement influences protein structure and enhances thermal protein stability, *Protein Sci.* 10 (2) (2001) 250–261.
- [41] I.M. Kuznetsova, K.K. Turoverov, V.N. Uversky, What macromolecular crowding can do to a protein, *Int. J. Mol. Sci.* 15 (12) (2014) 23090–23140.
- [42] G. Ping, J.M. Yuan, Z. Sun, Y. Wei, Studies of effects of macromolecular crowding and confinement on protein folding and protein stability, *J. Mol. Recognit.* 17 (5) (2004) 433–440.
- [43] D.M. Hatters, A.P. Minton, G.J. Howlett, Macromolecular crowding accelerates amyloid formation by human apolipoprotein C-II, *J. Biol. Chem.* 277 (10) (2002) 7824–7830.
- [44] B. Van den Berg, R.J. Ellis, C.M. Dobson, Effects of macromolecular crowding on protein folding and aggregation, *EMBO J.* 18 (24) (1999) 6927–6933.
- [45] L.A. Munishkina, E.M. Cooper, V.N. Uversky, A.L. Fink, The effect of macromolecular crowding on protein aggregation and amyloid fibril formation, *J. Mol. Recognit.* 17 (5) (2004) 456–464.
- [46] M. Bokvist, G. Grobner, Misfolding of amyloidogenic proteins at membrane surfaces: the impact of macromolecular crowding, *J. Am. Chem. Soc.* 129 (48) (2007) 14848–14849.
- [47] Z. Zhou, J.B. Fan, H.L. Zhu, F. Shewmaker, X. Yan, X. Chen, J. Chen, G.F. Xiao, L. Guo, Y. Liang, Crowded cell-like environment accelerates the nucleation step of amyloidogenic protein misfolding, *J. Biol. Chem.* 284 (44) (2009) 30148–30158.
- [48] X.D. Luo, F.L. Kong, H.B. Dang, J. Chen, Y. Liang, Macromolecular crowding favors the fibrillization of beta2-microglobulin by accelerating the nucleation step and inhibiting fibril disassembly, *Biochim. Biophys. Acta* 1864 (11) (2016) 1609–1619.
- [49] F. Librizzi, V. Fodera, V. Vetri, C. Lo Presti, M. Leone, Effects of confinement on insulin amyloid fibrils formation, *Eur. Biophys. J.* 36 (7) (2007) 711–715.
- [50] R.J. Ellis, Macromolecular crowding: an important but neglected aspect of the intracellular environment, *Curr. Opin. Struct. Biol.* 11 (1) (2001) 114–119.
- [51] N.C. Shirai, M. Kikuchi, The interplay of intrinsic disorder and macromolecular crowding on alpha-synuclein fibril formation, *J. Chem. Phys.* 144 (5) (2016) 055101.
- [52] F. Musiani, A. Giorgetti, Protein aggregation and molecular crowding: perspectives from multiscale simulations, *Int. Rev. Cell Mol. Biol.* 329 (2017) 49–77.
- [53] M. Gao, R. Winter, The effects of lipid membranes, crowding and osmolytes on the aggregation, and fibrillation propensity of human IAPP, *J. Diabetes Res.* 2015 (2015) 849017.
- [54] R. Crespo, E. Villar-Alvarez, P. Taboada, F.A. Rocha, A.M. Damas, P.M. Martins, Insoluble off-pathway aggregates as crowding agents during amyloid fibril formation, *J. Phys. Chem. B* 121 (10) (2017) 2288–2298.
- [55] J. Liu, F.C. Dehle, Y. Liu, E. Bahraminejad, H. Ecroyd, D.C. Thorn, J.A. Carver, The effect of milk constituents and crowding agents on amyloid fibril formation by kappa-casein, *J. Agric. Food Chem.* 64 (6) (2016) 1335–1343.
- [56] R. Berwick, D.J. Vaux, L. Jean, Multiphasic effect of vinyl pyrrolidone polymers on amyloidogenesis, from macromolecular crowding to inhibition, *Biochem. J.* 475 (21) (2018) 3417–3436.
- [57] C.G. Glabe, Structural classification of toxic amyloid oligomers, *J. Biol. Chem.* 283 (44) (2008) 29639–29643.
- [58] A. Dubnovitsky, A. Sandberg, M.M. Rahman, I. Benilova, C. Lendel, T. Hard, Amyloid-beta protofibrils: size, morphology and synaptotoxicity of an engineered mimic, *PLoS ONE* 8 (7) (2013) e66101.
- [59] P. Cizas, R. Budvytyte, R. Morkuniene, R. Moldovan, M. Broccio, M. Losche, G. Niaura, G. Valincius, V. Borutaite, Size-dependent neurotoxicity of beta-amyloid oligomers, *Arch. Biochem. Biophys.* 496 (2) (2010) 84–92.
- [60] S. Lee, E.J. Fernandez, T.A. Good, Role of aggregation conditions in structure, stability, and toxicity of intermediates in the Abeta fibril formation pathway, *Protein Sci.* 16 (4) (2007) 723–732.
- [61] M. Ahmed, J. Davis, D. Aucoin, T. Sato, S. Ahuja, S. Aimoto, J.I. Elliott, W.E. Van Nostrand, S.O. Smith, Structural conversion of neurotoxic amyloid-beta(1–42) oligomers to fibrils, *Nat. Struct. Mol. Biol.* 17 (5) (2010) 561–567.
- [62] M. Verma, A. Vats, V. Taneja, Toxic species in amyloid disorders: oligomers or mature fibrils, *Ann. Indian Acad. Neurol.* 18 (2) (2015) 138–145.
- [63] B. Keshet, J.J. Gray, T.A. Good, Structurally distinct toxicity inhibitors bind at common loci on beta-amyloid fibril, *Protein Sci.* 19 (12) (2010) 2291–2304.
- [64] A. Lorenzo, B.A. Yankner, Amyloid fibril toxicity in Alzheimer's disease and diabetes, *Ann. N. Y. Acad. Sci.* 777 (1) (1996) 89–95.

- [65] C. Wu, H. Lei, Z. Wang, W. Zhang, Y. Duan, Phenol red interacts with the protofibril-like oligomers of an amyloidogenic hexapeptide NFGAIL through both hydrophobic and aromatic contacts, *Biophys. J.* 91 (10) (2006) 3664–3672.
- [66] A.A. Reyes Barcelo, F.J. Gonzalez-Velasquez, M.A. Moss, Soluble aggregates of the amyloid-beta peptide are trapped by serum albumin to enhance amyloid-beta activation of endothelial cells, *J Biol Eng* 3 (2009) 5.
- [67] P.A. Weber, H.C. Chang, K.E. Spaeth, J.M. Nitsche, B.J. Nicholson, The permeability of gap junction channels to probes of different size is dependent on connexin composition and permeant-pore affinities, *Biophys. J.* 87 (2) (2004) 958–973.
- [68] P. Sengupta, K. Garai, J. Balaji, N. Periasamy, S. Maiti, Measuring Size Distribution in Highly Heterogeneous Systems with Fluorescence Correlation Spectroscopy, *Biophys. J.* 84 (3) (2003) 1977–1984.
- [69] M. Amaro, T. Wellbrock, D.J.S. Birch, O.J. Rolinski, Inhibition of beta-amyloid aggregation by fluorescent dye labels, *Appl. Phys. Lett.* 104 (6) (2014) 063704.
- [70] S.P. Zustiak, S. Pubill, A. Ribeiro, J.B. Leach, Hydrolytically degradable poly(ethylene glycol) hydrogel scaffolds as a cell delivery vehicle: characterization of PC12 cell response, *Biotechnol. Prog.* 29 (5) (2013) 1255–1264.
- [71] M. Novo, S. Freire, W. Al-Soufi, Critical aggregation concentration for the formation of early Amyloid-beta (1–42) oligomers, *Sci. Rep.* 8 (1) (2018) 1783.
- [72] J. Waters, The concentration of soluble extracellular amyloid-beta protein in acute brain slices from CRND8 mice, *PLoS ONE* 5 (12) (2010) e15709.
- [73] E. Karran, M. Mercken, B. De Strooper, The amyloid cascade hypothesis for Alzheimer's disease: an appraisal for the development of therapeutics, *Nat. Rev. Drug Discov.* 10 (9) (2011) 698–712.
- [74] J. Cummings, G. Lee, T. Mortsdorf, A. Ritter, K. Zhong, Alzheimer's disease drug development pipeline: 2017, *Alzheimers Dement (N Y)* 3 (3) (2017) 367–384.
- [75] J. Cummings, T. Morstorf, G. Lee, Alzheimer's drug-development pipeline: 2016, *Alzheimers Dement (N Y)* 2 (4) (2016) 222–232.
- [76] S. Gilman, M. Koller, R.S. Black, L. Jenkins, S.G. Griffith, N.C. Fox, L. Eisner, L. Kirby, M.B. Rovira, F. Forette, J.M. Orgogozo, A.N.S. Team, Clinical effects of Abeta immunization (AN1792) in patients with AD in an interrupted trial, *Neurology* 64 (9) (2005) 1553–1562.
- [77] C. Holmes, D. Boche, D. Wilkinson, G. Yadegarfar, V. Hopkins, A. Bayer, R.W. Jones, R. Bullock, S. Love, J.W. Neal, E. Zotova, J.A.R. Nicoll, Long-term effects of A $\beta$ 42 immunisation in Alzheimer's disease: follow-up of a randomised, placebo-controlled phase I trial, *The Lancet* 372 (9634) (2008) 216–223.
- [78] T. Tabira, Immunization therapy for alzheimer disease: a comprehensive review of active immunization strategies, *Tohoku J. Exp. Med.* 220 (2) (2010) 95–106.
- [79] D.A. Drachman, The amyloid hypothesis, time to move on: amyloid is the downstream result, not cause, of Alzheimer's disease, *Alzheimers Dement* 10 (3) (2014) 372–380.
- [80] A.J. Engler, S. Sen, H.L. Sweeney, D.E. Discher, Matrix elasticity directs stem cell lineage specification, *Cell* 126 (4) (2006) 677–689.
- [81] L.M. Postovit, E.A. Seftor, R.E. Seftor, M.J. Hendrix, A three-dimensional model to study the epigenetic effects induced by the microenvironment of human embryonic stem cells, *Stem Cells* 24 (3) (2006) 501–505.
- [82] M. Cavo, M. Caria, I. Pulsoni, F. Beltrame, M. Fato, S. Scaglione, A new cell-laden 3D Alginate-Matrigel hydrogel resembles human breast cancer cell malignant morphology, spread and invasion capability observed "in vivo", *Sci. Rep.* 8 (1) (2018) 5333.
- [83] M. Mirbagheri, V. Adibnia, B.R. Hughes, S.D. Waldman, X. Banquy, D.K. Hwang, Advanced cell culture platforms: a growing quest for emulating natural tissues, *Mater Horiz* 6 (1) (2019) 45–71.
- [84] S. Sadri, M. Khazaei, A. Ghanbari, M.R. Khazaei, P. Shah, Neuronal differentiation of PC12 and embryonic stem cells in two- and three-dimensional in vitro culture, *Indian J. Exp. Biol.* 52 (4) (2014) 305–311.
- [85] S. Matsumura, K. Shinoda, M. Yamada, S. Yokojima, M. Inoue, T. Ohnishi, T. Shimada, K. Kikuchi, D. Masui, S. Hashimoto, M. Sato, A. Ito, M. Akioka, S. Takagi, Y. Nakamura, K. Nemoto, Y. Hasegawa, H. Takamoto, H. Inoue, S. Nakamura, Y. Nabeshima, D.B. Teplow, M. Kinjo, M. Hoshi, Two distinct amyloid beta-protein (Abeta) assembly pathways leading to oligomers and fibrils identified by combined fluorescence correlation spectroscopy, morphology, and toxicity analyses, *J. Biol. Chem.* 286 (13) (2011) 11555–11562.
- [86] J.X. Lu, W. Qiang, W.M. Yau, C.D. Schwieters, S.C. Meredith, R. Tycko, Molecular structure of beta-amyloid fibrils in Alzheimer's disease brain tissue, *Cell* 154 (6) (2013) 1257–1268.
- [87] T.M. Ryan, J. Caine, H.D. Mertens, N. Kirby, J. Nigro, K. Breheney, L.J. Waddington, V.A. Streltsov, C. Curtain, C.L. Masters, B.R. Roberts, Ammonium hydroxide treatment of Abeta produces an aggregate free solution suitable for biophysical and cell culture characterization, *PeerJ* 1 (2013) e73.
- [88] K.A. Coalier, G.S. Paranjape, S. Karki, M.R. Nichols, Stability of early-stage amyloid-beta(1–42) aggregation species, *Biochim. Biophys. Acta* 1834 (1) (2013) 65–70.
- [89] A. Zhang, W. Qi, T.A. Good, E.J. Fernandez, Structural differences between Abeta(1–40) intermediate oligomers and fibrils elucidated by proteolytic fragmentation and hydrogen/deuterium exchange, *Biophys. J.* 96 (3) (2009) 1091–1104.
- [90] Y. Zhang, D.L. Rempel, J. Zhang, A.K. Sharma, L.M. Mirica, M.L. Gross, Pulsed hydrogen-deuterium exchange mass spectrometry probes conformational changes in amyloid beta (Abeta) peptide aggregation, *Proc Natl Acad Sci U.S.A.* 110 (36) (2013) 14604–14609.
- [91] K. Broersen, F. Rousseau, J. Schymkowitz, The culprit behind amyloid beta peptide related neurotoxicity in Alzheimer's disease: oligomer size or conformation? *Alzheimers Res Ther* 2 (4) (2010) 12.
- [92] S.S. Wang, A. Becerra-Arteaga, T.A. Good, Development of a novel diffusion-based method to estimate the size of the aggregated Abeta species responsible for neurotoxicity, *Biotechnol. Bioeng.* 80 (1) (2002) 50–59.
- [93] T. Luhrs, C. Ritter, M. Adrian, D. Riek-Loher, B. Bohrmann, H. Dobeli, D. Schubert, R. Riek, 3D structure of Alzheimer's amyloid-beta(1–42) fibrils, *Proc Natl Acad Sci U.S.A.* 102 (48) (2005) 17342–17347.
- [94] J. Seeliger, A. Werkmuller, R. Winter, Macromolecular crowding as a suppressor of human IAPP fibril formation and cytotoxicity, *PLoS ONE* 8 (7) (2013) e69652.
- [95] H.X. Zhou, G. Rivas, A.P. Minton, Macromolecular crowding and confinement: biochemical, biophysical, and potential physiological consequences, *Annu. Rev. Biophys.* 37 (2008) 375–397.
- [96] H.X. Zhou, Protein folding in confined and crowded environments, *Arch. Biochem. Biophys.* 469 (1) (2008) 76–82.
- [97] L.W. Simpson, G.L. Szeto, H. Boukari, T.A. Good, J.B. Leach, Impact of four common hydrogels on amyloid- $\beta$  (A $\beta$ ) aggregation and cytotoxicity: implications for 3D models of Alzheimer's disease, *ACS Omega* (2019) Manuscript in review.
- [98] Y.L. Yang, L.M. Leone, L.J. Kaufman, Elastic moduli of collagen gels can be predicted from two-dimensional confocal microscopy, *Biophys. J.* 97 (7) (2009) 2051–2060.
- [99] P. Banerjee, D. Lenz, J.P. Robinson, J.L. Rickus, A.K. Bhunia, A novel and simple cell-based detection system with a collagen-encapsulated B-lymphocyte cell line as a biosensor for rapid detection of pathogens and toxins, *Lab. Invest.* 88 (2) (2008) 196–206.
- [100] S. Kota, S. Hou, W. Guarrant, F. Madoux, S. Troutman, V. Fernandez-Vega, N. Alekseeva, N. Madala, L. Scampavia, J. Kissil, T.P. Spicer, A novel three-dimensional high-throughput screening approach identifies inducers of a mutant KRAS selective lethal phenotype, *Oncogene* 37 (32) (2018) 4372–4384.
- [101] G. Vlachogiannis, S. Hedayat, A. Vatsiou, Y. Jamin, J. Fernandez-Mateos, K. Khan, A. Lampis, K. Eason, I. Huntingford, R. Burke, M. Rata, D.M. Koh, N. Tunariu, D. Collins, S. Hukli-Wilson, C. Ragulan, I. Spiteri, S.Y. Moorcraft, I. Chau, S. Rao, D. Watkins, N. Fotiadis, M. Bali, M. Darvish-Damavandi, H. Lote, Z. Eltahir, E.C. Smyth, R. Begum, P.A. Clarke, J.C. Hahne, M. Dowsett, J. de Bono, P. Workman, A. Sadanandam, M. Fassan, O.J. Sansom, S. Eccles, N. Starling, C. Braconi, A. Sottoriva, S.P. Robinson, D. Cunningham, N. Valeri, Patient-derived organoids model treatment response of metastatic gastrointestinal cancers, *Science* 359 (6378) (2018) 920–926.
- [102] J. Kondo, T. Ekawa, H. Endo, K. Yamazaki, N. Tanaka, Y. Kukita, H. Okuyama, J. Okami, F. Imamura, M. Ohue, K. Kato, T. Nomura, A. Kohara, S. Mori, S. Dan, M. Inoue, High-throughput screening in colorectal cancer tissue-originated spheroids, *Cancer Sci.* 110 (1) (2019) 345–355.
- [103] N. Phan, J.J. Hong, B. Tofig, M. Mapua, D. Elashoff, N.A. Moatamed, J. Huang, S. Memarzadeh, R. Damoiseaux, A. Soragni, A simple high-throughput approach identifies actionable drug sensitivities in patient-derived tumor organoids, *Commun. Biol.* 2 (2019) 78.
- [104] M. van de Wetering, H.E. Francies, J.M. Francis, G. Bounova, F. Iorio, A. Pronk, W. van Houdt, J. van Gorp, A. Taylor-Weiner, L. Kester, A. McLaren-Douglas, J. Blokter, S. Jaksani, S. Bartfeld, R. Volckman, P. van Sluis, V.S. Li, S. Seepo, C. Sekhar Pedamallu, K. Cibulskis, S.L. Carter, A. McKenna, M.S. Lawrence, L. Lichtenstein, C. Stewart, J. Koster, R. Versteeg, A. van Oudenaarden, J. Saez-Rodriguez, R.G. Vries, G. Getz, L. Wessels, M.R. Stratton, U. McDermott, M. Meyerson, M.J. Garnett, H. Clevers, Prospective derivation of a living organoid biobank of colorectal cancer patients, *Cell* 161 (4) (2015) 933–945.
- [105] Screening in 3D, Bayer Scientific Magazine Research, 2014, pp. 6–9.
- [106] C. Bioarray, PDO-based Drug Screening. <<https://www.creative-bioarray.com/pdo-based-drug-screening.htm>> Accessed 2020.